Introduction

Waveform inversion (WI) is a methodology for velocity model building using seismic wavefields (Tarantola, 1984; Woodward, 1992; Pratt, 1999; Sirgue and Pratt, 2004; Plessix, 2006; Vigh and Starr, 2008; Plessix, 2009; Symes, 2009). This technique is regarded as one of the costliest for velocity estimation, but it is gaining momentum due to its accuracy and to significant increase in compute power.

The essential building block of WI is wavefield simulation using a wave-equation, often the constant density acoustic wave-equation. WI is normally implemented in the data-domain, by updating the model to match the simulated and recorded data. This match requires the strong assumption that the chosen wave-equation is consistent with the physics of wave propagation in the earth, which is not likely to be the case when the earth is characterized by strong (poro)elastic effects. Thus, a significant part of WI is often directed toward removing the components of the observed data that are inconsistent with the assumptions made about the wave-equation.

Another key component of WI is the objective function (OF) used to measure the match between the simulated and recorded data. The OF is assumed to be more-or-less convex, thus enabling its minimization using gradient-based techniques. A successful implementation of WI requires a fast and accurate implementation of the OF gradient.

An effective gradient calculation is based on the adjoint state method (Plessix, 2006; Symes, 2009). In summary, this method consists of the following steps: (1) compute the *state variables*, i.e. the seismic wavefields obtained from the source by forward modeling; (2) compute the *adjoint source*, i.e. a calculation based on the OF and on the state variables; (3) compute the *adjoint state variables*, i.e. the seismic wavefields obtained from the adjoint source by backward modeling; (4) compute the *gradient* using the state and adjoint state variables.

WI could be implemented in the data-domain or in the image domain. Here, we concentrate on the WI implementation in the image-domain, as suggested by Symes (2009). The data- and image-domains implementations are not different in their use of seismic wavefields, but merely in their implementation of the OF gradient when multiple seismic experiments (e.g. shots) are considered. We present a comparative derivation of the data-domain and image-domain implementations and illustrate the less common image-domain method with a synthetic example.

Waveform inversion

The state variables for the adjoint state method are obtained by solving the acoustic wave-equation

$$\mathcal{L}\left(\mathbf{x},\omega,m\right)u_s\left(\mathbf{e},\mathbf{x},\omega\right)=f_s\left(\mathbf{e},\mathbf{x},\omega\right)\ , \tag{1}$$

where $\mathcal{L}$ denotes the wave operator, u_s is the simulated wavefield, f_s is the source data, m are the model parameters (velocity or slowness), $\mathbf{e}$ is the experiment index, ω is the frequency, and $\mathbf{x}$ are the space coordinates $\{x,y,z\}$.

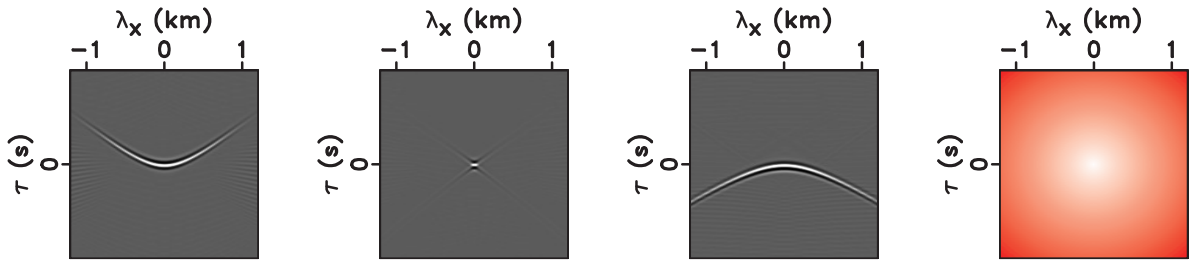
Conventional WI is an inverse problem with the model found by minimizing an OF defined using the difference between the observed and simulated wavefields, u_o and u_s (Tarantola, 1984; Pratt, 1999):

$$\mathcal{H}=\sum_{\mathbf{e}}\frac{1}{2}\|K_D\left(\mathbf{e},\mathbf{x}\right)\left(u_s\left(\mathbf{e},\mathbf{x},\omega\right)-u_o\left(\mathbf{e},\mathbf{x},\omega\right)\right)\|^2_{\mathbf{x},\omega}\ . \tag{2}$$

Here, $K_D\left(\mathbf{e},\mathbf{x}\right)$ is a mask operator which limits the definition of the OF to specific locations, e.g. to positions on the surface. This common objective function suffers, among other things, from cycle skipping due to the oscillatory nature of the subtracted wavefields. This problem is usually addressed by bootstrapping the frequency from low to high (Sirgue and Pratt, 2004).

A similar procedure can be implemented in the image-domain with extended images obtained by wave-equation migration (downward continuation or reverse-time), using the extended imaging condition (Rickett and Sava, 2002; Sava and Fomel, 2006; Sava and Vasconcelos, 2011). The state variables are represented by the source and receiver wavefields, u_s and u_r, simulated using the source wavelet f_s and the recorded data f_r:

$$\begin{bmatrix}\mathcal{L}\left(\mathbf{x},\omega,m\right) & 0\\ 0 & \mathcal{L}^*\left(\mathbf{x},\omega,m\right)\end{bmatrix}\begin{bmatrix}u_s\left(\mathbf{e},\mathbf{x},\omega\right)\\ u_r\left(\mathbf{e},\mathbf{x},\omega\right)\end{bmatrix}=\begin{bmatrix}f_s\left(\mathbf{e},\mathbf{x},\omega\right)\\ f_r\left(\mathbf{e},\mathbf{x},\omega\right)\end{bmatrix}\ . \tag{3}$$



(a) (b) (c) (d)

Figure 1: Extended images for a horizontal reflector imaged with (a) low, (b) correct and (c) high velocities. Panel (d) depicts the penalty function used in the image-domain OF.

The wavefields u_s and u_r are obtained by forward and backward modeling, respectively. In this case, we can formulate the OF as

$$\mathcal{H}_I = \frac{1}{2}\| K_I\left(\mathbf{x}\right) P\left(\boldsymbol{\lambda},\tau\right) r\left(\mathbf{x},\boldsymbol{\lambda},\tau\right) \|^2_{\mathbf{x},\boldsymbol{\lambda},\tau} \ , \tag{4}$$

where r are extended images, Figure 1(a)-1(c), whose characteristics depend on the accuracy of the model (Sava and Vasconcelos, 2011)

$$r\left(\mathbf{x},\boldsymbol{\lambda},\tau\right) = \sum_{\mathbf{e}}\sum_{\omega} \overline{u_s\left(\mathbf{e},\mathbf{x}-\boldsymbol{\lambda},\omega\right)} u_r\left(\mathbf{e},\mathbf{x}+\boldsymbol{\lambda},\omega\right) e^{2i\omega\tau} \ , \tag{5}$$

$K_I\left(\mathbf{x}\right)$ is a mask operator which restricts the evaluation of the OF to some locations in the image, and $P\left(\boldsymbol{\lambda},\tau\right)$ is a penalty operator applied in the extended space, Figure 1(d). Then, we compute the gradient of the OF by defining adjoint sources (Yang and Sava, 2011)

$$\begin{bmatrix} g_s\left(\mathbf{e},\mathbf{x},\omega\right) \\ g_r\left(\mathbf{e},\mathbf{x},\omega\right) \end{bmatrix} = \begin{bmatrix} \frac{\partial \mathcal{H}_I}{\partial u_s} \\ \frac{\partial \mathcal{H}_I}{\partial u_r} \end{bmatrix} = \begin{bmatrix} K_I\overline{K_I}\sum\limits_{\tau,\boldsymbol{\lambda}} P\overline{P}\ \Re\left[r\left(\mathbf{x},\boldsymbol{\lambda},\tau\right) \overline{u_r\left(\mathbf{e},\mathbf{x},\omega\right)} e^{-2i\omega\tau} \right] \\ K_I\overline{K_I}\sum\limits_{\tau,\boldsymbol{\lambda}} P\overline{P}\ \Re\left[r\left(\mathbf{x},\boldsymbol{\lambda},\tau\right) u_s\left(\mathbf{e},\mathbf{x},\omega\right) e^{-2i\omega\tau} \right] \end{bmatrix} \ , \tag{6}$$

computing the adjoint state variables, a_s (backward modeling) and a_r (forward modeling),

$$\begin{bmatrix} \mathcal{L}^*\left(\mathbf{x},\omega,m\right) & 0 \\ 0 & \mathcal{L}\left(\mathbf{x},\omega,m\right) \end{bmatrix} \begin{bmatrix} a_s\left(\mathbf{e},\mathbf{x},\omega\right) \\ a_r\left(\mathbf{e},\mathbf{x},\omega\right) \end{bmatrix} = \begin{bmatrix} g_s\left(\mathbf{e},\mathbf{x},\omega\right) \\ g_r\left(\mathbf{e},\mathbf{x},\omega\right) \end{bmatrix} \ , \tag{7}$$

and evaluating the gradient of the constrained (augmented) OF (Plessix, 2006) by the correlation of the state (u_s, u_r) and adjoint state variables (a_s, a_r)

$$\frac{\partial \mathcal{A}_I}{\partial m}\left(\mathbf{x}\right) = \sum_{\mathbf{e}}\sum_{\omega} \omega^2 \left(\overline{u_s\left(\mathbf{e},\mathbf{x},\omega\right)} a_s\left(\mathbf{e},\mathbf{x},\omega\right) + \overline{u_r\left(\mathbf{e},\mathbf{x},\omega\right)} a_r\left(\mathbf{e},\mathbf{x},\omega\right) \right) \ . \tag{8}$$

Example

Figures 2(a)-2(l) illustrate the methodology with the Marmousi model. Figures 2(a)-2(d) correspond to the starting model. The conventional image 2(a) constructed using the background model 2(b) is used to pick locations where extended gathers are constructed. The space-lag CIGs 2(c) and angle gathers 2(d) indicate the inaccuracy of the starting model. Figures 2(e)-2(h) correspond to the updated model after 20 iterations of non-linear inversion, which are sufficient to decrease the objective function to negligible values, Figure 3. As for the background model, the conventional image 2(e) is built using the updated model 2(f). The space-lag CIGs 2(g) and angle gathers 2(h) indicate that the model has been correctly updated. For comparison, Figures 2(i)-2(l) correspond to the correct model. In this case the gathers are as flat as for the updated model, indicating that the main features of the velocity model are resolved by the inversion and no further updates can be accomplished through the analysis of the extended gathers.

We note that the points at which extended images are computed change with iterations, as seen in Figures 2(a)-2(e)-2(i). We also note that the space-lag CIGs and the angle gathers are used only to illustrate the accuracy of the model, and not for the wavefield tomography.

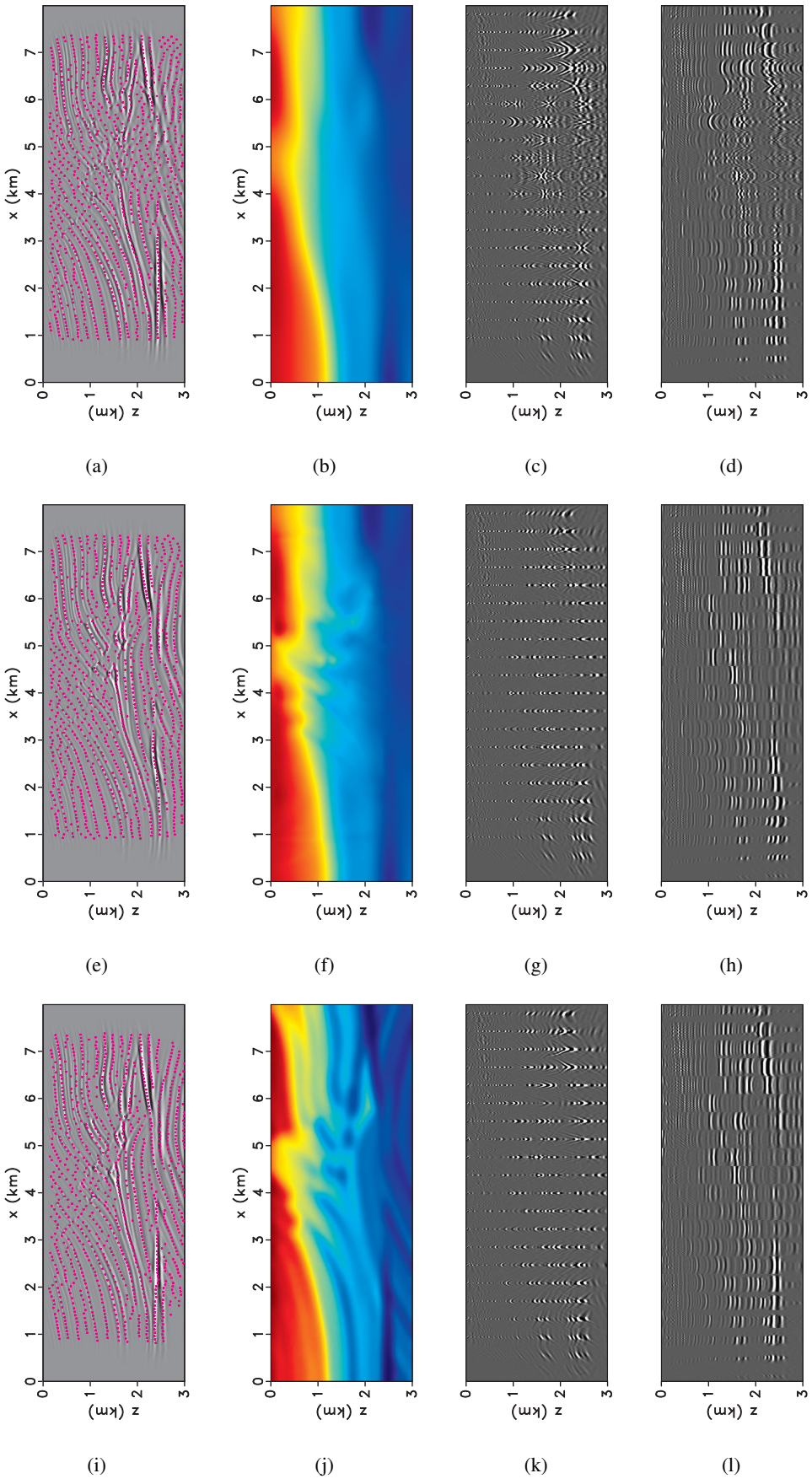


Figure 2: Conventional images (a-e-i), velocity models (b-f-j), space-lag gathers (c-g-k) and angle gathers (d-h-l) for the starting, updated and correct models, from top to bottom.

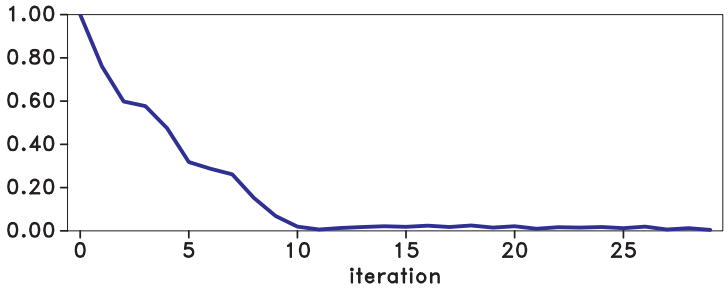


Figure 3: Image-domain objective function as a function of iteration number.

Conclusions

WI can be formulated both in the data-domain or in the image-domain. The same wavefields are used in both cases (i.e. the same wave-equation, the same sources and boundary conditions, etc), therefore these implementations are not at all different from this point of view. The image-domain OF applies a penalty function depending on space- and time-lags to the correlation of the source and receiver wavefields after summation over experiments, i.e. it exploits the semblance principle. This OF uses correlations at any locations in the image, including surface locations. This technique works for any type of seismic experiment (point source, plane source, etc) and the wavefield reconstruction can be implemented equally well in the time-domain or in the frequency-domain. No cumbersome time-lag picking is necessary to define the image-domain objective function.

Acknowledgments

We acknowledge the sponsors of the Center for Wave Phenomena at Colorado School of Mines. The reproducible numeric examples use the Madagascar open-source package (http://www.reproducibility.org).

REFERENCES

Plessix, R.-E., 2006, A review of the adjoint state method for computing the gradient of a functional with geophysical applications: Geophysical Journal International, **167**, 495–503.

———, 2009, Three-dimensional frequency-domain full-waveform inversion with an iterative solver: Geophysics, **74**, WCC53–WCC61.

Pratt, R. G., 1999, Seismic waveform inversion in the frequency domain, Part 1: Theory and verification in a physical scale model: Geophysics, **64**, 888–901.

Rickett, J., and P. Sava, 2002, Offset and angle-domain common image-point gathers for shot-profile migration: Geophysics, **67**, 883–889.

Sava, P., and S. Fomel, 2006, Time-shift imaging condition in seismic migration: Geophysics, **71**, S209–S217.

Sava, P., and I. Vasconcelos, 2011, Extended imaging condition for wave-equation migration: Geophysical Prospecting, **59**, 35–55.

Sirgue, L., and R. Pratt, 2004, Efficient waveform inversion and imaging: A strategy for selecting temporal frequencies: Geophysics, **69**, 231–248.

Symes, W., 2009, Migration velocity analysis and waveform inversion: Geophysical Prospecting, **56**, 765–790.

Tarantola, A., 1984, Inversion of seismic reflection data in the acoustic approximation: Geophysics, **49**, 1259–1266.

Vigh, D., and E. W. Starr, 2008, 3D prestack plane-wave, full-waveform inversion: Geophysics, **73**, VE135–VE144.

Woodward, M. J., 1992, Wave-equation tomography: Geophysics, **57**, 15–26.

Yang, T., and P. Sava, 2011, Waveform inversion in the image domain: Presented at the 73rd Mtg., Abstracts, Eur. Assoc. Expl. Geophys.